Monosaccharide-Linked Inhibitors of O^6-Methylguanine-DNA Methyltransferase (MGMT): Synthesis, Molecular Modeling, and Structure−Activity Relationships

Jost Reinhard,[†] William E. Hull,[‡] Claus-Wilhelm von der Lieth,[‡] Uta Eichhorn,[§] Hans-Christian Kliem,[†] Bernd Kaina,[‡] and Manfred Wiessler*,[†]

Division of Molecular Toxicology and Central Spectroscopy Department, German Cancer Research Center, Postfach 101949, D-69009 Heidelberg, Germany, and Division of Applied Toxicology, Institute of Toxicology, University of Mainz, Obere Zahlbacher Strasse 67, D-55131 Mainz, Germany

Received January 5, 2001

A series of potential inhibitors of the human DNA repair protein O^6-methylguanine-DNA methyltransferase (MGMT) were synthesized, characterized in detail by NMR, and tested for their ability to deplete MGMT activity in vitro. The new compounds, ω-[O^6-*R*-guan-9-yl]-$(CH_2)_n$-β-d-glucosides with R = benzyl or 4-bromothenyl and $\omega = n = 2, 4, \ldots 12$, were compared with the established inhibitors O^6-benzylguanine (O^6-BG), 8-aza-O^6-benzylguanine (8-aza-BG), and O^6-(4-bromothenyl)guanine (4-BTG), which exhibit in an in vitro assay IC_{50} values of 0.62, 0.038, and 0.009 μM, respectively. Potential advantages of the glucosides are improved water solubility and selective uptake in tumor cells. The 4-BTG glucosides with n = 2, 4, 6 show moderate inhibition with an IC_{50} of ca. 0.5 μM, while glucosides derived from BG and 8-aza-BG showed significantly poorer inhibition compared to the parent compounds. The 4-BTG glucosides with n = 8, 10, 12 were effective inhibitors with IC_{50} values of ca. 0.03 μM. To understand this behavior, extensive molecular modeling studies were performed using the published crystal structure of MGMT (PDB entry: 1QNT). The inhibitor molecules were docked into the BG binding pocket, and molecular dynamics simulations with explicit water molecules were carried out. Stabilization energies for the interactions of specific regions of the inhibitor and individual amino acid residues were calculated. The alkyl spacer is located in a cleft along helix 6 of MGMT. With increasing spacer length there is increasing interaction with several amino acid residues which play an important role in the proposed nucleotide flipping mechanism required for DNA repair.

Introduction

The human DNA repair protein O^6-methylguanine-DNA methyltransferase (MGMT) plays a critical role in cancer therapy with alkylating reagents such as alkyl nitrosoureas and alkyl triazenes. Among the resulting DNA adducts, O^6-alkylguanines are considered to be of major importance for the induction of cancer, mutation, and cell death. These adducts direct the incorporation of either thymine or cytosine without blocking DNA replication, resulting in GC to AT transition mutations. MGMT provides protection against such lesions by removing the O^6-alkyl adduct and transferring it to a cysteine acceptor group within the enzymes's active site.[1−4] The resulting MGMT-thioether is not reactivated; instead, the protein is ubiquitinated and degraded. Thus, MGMT is considered to be a suicide enzyme since the transfer is not reversible and activity can be recovered only by *de novo* protein synthesis. Consequently, tumor cells and neoplastic tissue with elevated MGMT levels can be resistant to alkylating therapeutics but can be resensitized by depletion of MGMT.[5−7] Derivatives of the free base guanine react as pseudosubstrates with MGMT and can completely abolish its activity.

Although potent inhibitors of MGMT have been found and introduced into adjuvant therapy,[4,8,9] they all have major disadvantages. In all cases no selectivity for neoplastic tissue has been achieved, leading to reduced repair capacity in normal tissue and loss of protection against the systemic side effects of chemotherapy. O^6-Benzylguanine (O^6-BG), a well-established inhibitor tested in phase I clinical trials,[10,11] exhibits poor water solubility, which limits its applications. Another very promising compound, 4-(benzyloxy)-2,6-diamino-5-nitrosopyrimidine,[9,12] has the disadvantage of a short half-life in vivo. The compounds 8-aza-O^6-benzylguanine and O^6-(4-bromothenyl)-guanine have IC_{50} values for MGMT inhibition which are, respectively, 3 times and 75 times lower than for O^6-BG.[8,9] However, these more potent inhibitors did not show tumor selectivity in animal testing.[13−15] To overcome these disadvantages, appropriate modifications in the pharmacophore are necessary.

Previously published results[6,8,9,16−20] indicate that basically only three positions in the purine core are suitable for structural variations, namely O,[6] C8, and N9. For example, specific modifications to substituents at O^6 or C8 may alter the electronic properties of the purine ring system and enhance the leaving ability of the alkyl group at O^6.[9,17] For modifications at N9, it is

* To whom correspondence should be addressed. Tel: +49-6221-423311. Fax: +49-6221-423375. E-mail: m.wiessler@dkfz.de.
[†] Division of Molecular Toxicology, German Cancer Research Center.
[‡] Central Spectroscopy Department, German Cancer Research Center.
[§] University of Mainz.

10.1021/jm010006e CCC: $20.00
Published on Web 10/31/2001

known that highly polar groups lead to a dramatic *decrease* in MGMT depletion activity, whereas bulky apolar groups do not hinder the ability to inhibit MGMT.[17,21] Not only substituent effects but also MGMT−DNA interactions can influence ligand affinity since DNA binding leads to steric hindrance of the competitive interaction with small-molecule inhibitors.[21]

A better understanding of the molecular mechanism of MGMT and structure−activity relationships for inhibitors can be obtained by computational approaches based on the available X-ray crystal structures of MGMT and biological data derived from in vitro studies. The first alkyltransferase (ATase) of the MGMT family to be crystallized was the 19 kDa C-terminal domain of the *ada* gene product from *Escherichia coli*.[22] Wibley et al.[23] reported the first homology model of the human protein based on the crystal structure of the *E. coli* ATase. A distortion of the DNA substrate was discussed and later specified in terms of the proposed flipping mechanism for the alkylated guanine,[24] based on descriptions of the analogous phenomenon for other methyltransferases.[25−28] Recently, the X-ray crystal structures of the human enzyme[29] and its benzylated and methylated products[30] have been determined. Although a homology model suggested a deeply buried active site, the crystal structure revealed that in the human protein the active site is reasonably accessible for pseudosubstrates. Site-directed mutagenesis studies indicated that several amino acid residues are involved in the MGMT reaction mechanism. The residues Arg128, Tyr114, and Lys165 were found to be necessary for DNA binding,[31−33] while Pro140, Gly156, Tyr158, and Gly160 proved to be essential for reaction with either O^6-BG or oligonucleotides containing O^6-methylguanine. Tyr114, conserved in all known sequences, was shown to play a key role in substrate specificity, DNA binding, and protection against mutations induced by methylating agents.[34] Cells expressing the K165A mutant of MGMT were still protected by the enzyme from the mutagenic effects of O^6-methylating agents and could not be sensitized by O^6-BG.[33] Similar results were obtained for various Gly156 mutants as well as for mutations at Cys150, Asn157, Tyr158, Ser159, Leu168, and Leu169.[31,35] At codon 160 mutations can lead to either increased sensitivity (G160A, G160W) or resistance toward O^6-BG (G160R and many others).[36] The mutants P140K and PVP(138-140)MLK showed a 10 000-fold decrease in sensitivity against O^6-BG.

Although data for purine-based inhibitors with substituents at N9 have been reported, the details of how the substituents influence activity have not been elucidated. Therefore, we have synthesized a set of such compounds to determine the required structural features of N9 substituents that are compatible with MGMT depletion. Glucosidation represents a general strategy for improving both drug solubility and targeting, two weaknesses of the inhibitors discussed above. For example, β-d-glucosylisophosphoramide mustard (Glu-IPM) exhibits in animal models the same therapeutic potency as isophosphoramide mustard but less systemic toxicity.[37] Glu-IPM is transported by SAAT1, an active, membrane-bound, sodium-dependent glucose cotransporter.[38] In tumors the expression of transport proteins for essential energy donors such as saccharides is enhanced. Glucose conjugates with antitumor activity, so-called "trojan horses", are accepted by SAAT1 and, therefore, accumulate preferentially in neoplastic tissue. Thus, appropriate glucosyl derivatives of MGMT inhibitors should provide *targeted* depletion of MGMT activity in neoplastic tissue and the desired reduction in MGMT-based therapy resistance while maintaining MGMT-based protection of normal tissue and minimizing toxicity.

To achieve this goal, it is essential to gain insight into the molecular structure requirements of MGMT inhibitors and the characteristics which lead to enhanced MGMT depletion. Since polar groups at purine N9 are unfavorable, we have introduced various [-O$(CH_2)_n$-] alkyl spacers between C1 of β-d-glucose and N9 of guanines bearing various O^6 substituents. Here we present the synthesis, purification, and spectroscopic characterization of these novel MGMT inhibitors. The results of initial in vitro inhibition assays are compared with interaction energies obtained from detailed molecular modeling studies of MGMT−inhibitor complexes. A detailed report concerning MGMT inhibition in tumor cell cultures is presented elsewhere.[39]

Results and Discussion

Synthesis. A series of protected alkyl-β-d-glucopyranosides (see Chart 1) was prepared according to step A in Chart 2. The alkyl group was activated for subsequent reaction by a bromine substituent in the ω position. Alkyl groups $(CH_2)_n$ were used as spacers with n = 2, 4, 6, 8, 10, 12 for compounds **1**−**6**. For compound **7** a 2-butynyl moiety was employed. It was necessary to protect the glucose hydroxyl groups with either acetyl or benzoyl substituents. Since these are lost under basic conditions, it was crucial to work in a water-free environment.

The guanine derivative **8** (O^6-benzyl) was synthesized from 6-chloroguanine using a standard method for O^6 substitution by nucleophilic replacement of the halogen.[40] Derivative **10** (O^6-(4-bromothenyl)) was prepared from 6-chloroguanine by an improved method introduced by McElhinney et al.,[8] whereby the chlorine is first replaced by a trimethylamino group to give a trimethylammonium salt. Subsequent displacement of this group by an alcoholate gives higher overall yields and can be performed at room temperature. The 8-aza analogue **9** (O^6-benzyl, 8-aza) was obtained by ring closure of 6-benzyloxy-2,3,5-triaminopyrimidine using nitrite under reductive conditions.[41,42]

The family of protected, halogen-activated alkyl-β-d-glucosides was then used to alkylate position N9 of the guanine derivatives (step B in Chart 2) to give the odd-numbered protected compounds **11**−**27**. Deprotection (step C in Chart 2) then led to the even-numbered unprotected glucosides **12**−**28**. A problem with this alkylation strategy is that N9 and N7 of the purines are attacked equally well by suitable electrophiles; however, N7-substituted MGMT inhibitors are inactive. To maximize the N9/N7 substitution ratio, lithium hydride was employed to activate the imidazole ring, as demonstrated by Kjellberg and Liljenberg.[43]

All isolated products were characterized in detail by spectroscopic methods as described in the Materials and

Chart 1. Synthesized Compounds

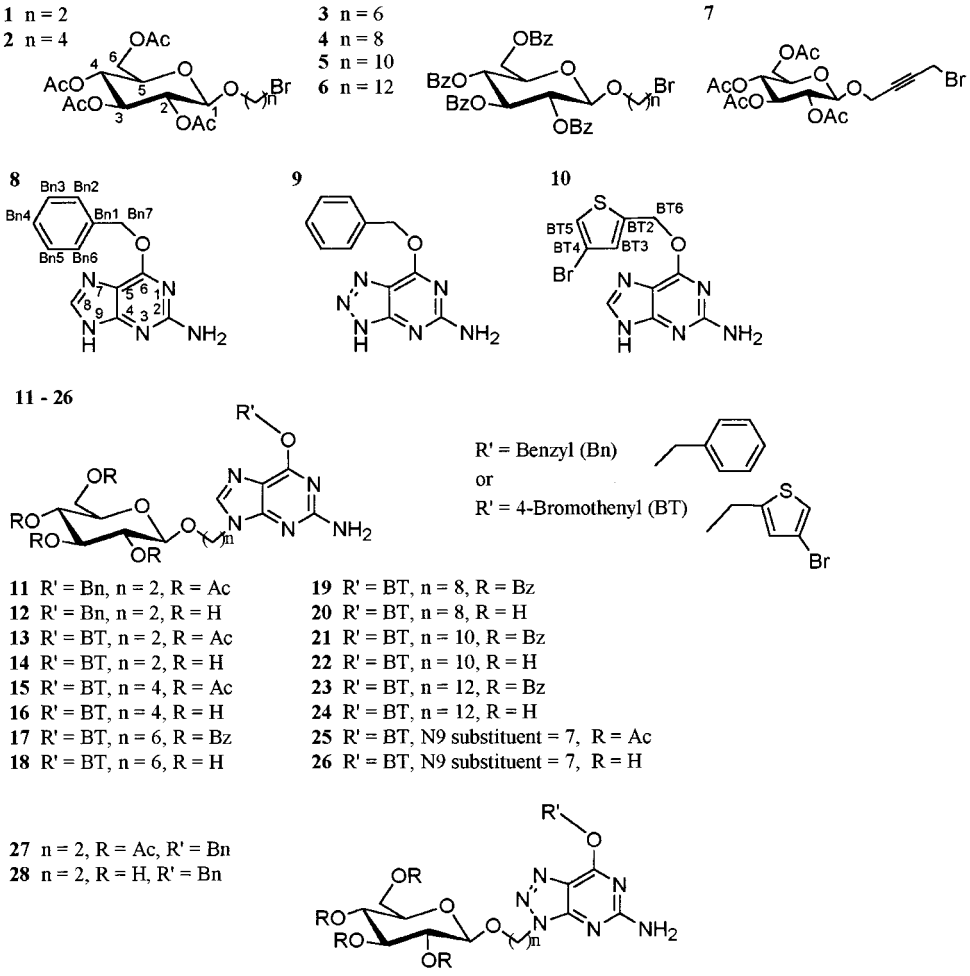

Chart 2. Reaction Schemes

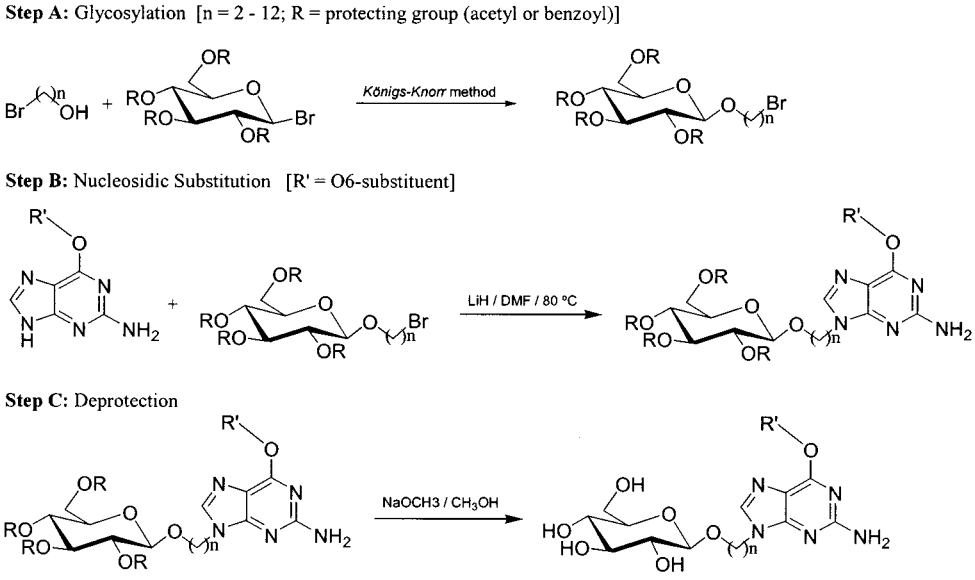

Methods. For the unprotected glucosides NMR studies were carried out at 11.7 T (500 MHz for ^{1}H) so that nearly complete and unambiguous assignments for all ^{1}H and ^{13}C resonances could be obtained for the complete family of inhibitors (provided as Supporting Information). NMR provided the only means for confirming the isomeric and stereochemical purity of the isolated compounds (β anomer, N9 vs N7 substitution).

The parallel synthesis of a family of glucosides allowed us to prepare the present set of guanine derivatives under a standardized set of conditions. Thus, this method is suitable for generating even larger libraries of analogous structures. Regarding purification by column and flash chromatography, we found that for the compounds with long spacers, such as **24**, there was no advantage in performing a purification of the pro-

Table 1. MGMT Depletion Assay Using Cell-Free Extracts from HeLa S3 Cells[a]

compound	IC_{50} [μM]
O^6-benzylguanine (**8**)	0.62
2-[O^6-benzylguan-9-yl]-ethyl-β-d-glucoside (**12**)	25.0
8-aza-O^6-benzylguanine (**9**)	0.038
2-[8-aza-O^6-benzylguan-9-yl]-ethyl-β-d-glucoside (**28**)	2.0
O^6-(4-bromothenyl)-guanine (**10**)	0.009
2-[O^6-(4-bromothenyl)-guan-9-yl]-ethyl-β-d-glucoside (**14**)	0.680
4-[O^6-(4-bromothenyl)-guan-9-yl]-butyl-β-d-glucoside (**16**)	0.450
6-[O^6-(4-bromothenyl)-guan-9-yl]-hexyl-β-d-glucoside (**18**)	0.450
8-[O^6-(4-bromothenyl)-guan-9-yl]-octyl-β-d-glucoside (**20**)	0.032
10-[O^6-(4-bromothenyl)-guan-9-yl]-decyl-β-d-glucoside (**22**)	0.030
12-[O^6-(4-bromothenyl)-guan-9-yl]-dodecyl-β-d-glucoside (**24**)	0.030
4-[O^6-(4-bromothenyl)-guan-9-yl]-but-2-ynyl-β-d-glucoside (**26**)	0.250

[a] Detailed inhibition studies are presented in ref 39.

tected glucoside; good separations were obtained with the deprotected compounds. However, for the shorter spacers (ethyl, butyl), it proved to be very difficult to separate the N9- and N7-derivatives (distinguishable by NMR) in the deprotected glucoside form; in these cases purification of the protected species was necessary and successful.

MGMT Inhibition. In a first round of synthesis the glucosides **12**, **14,** and **28** were prepared and compared with their corresponding parent guanines **8**, **10**, and **9** in terms of their ability to inactivate MGMT (Table 1). As expected from previous results, N9 alkylation of the guanine leads to an increase in IC_{50} (factor 40 for **12** vs **8**; factor 53 for **28** vs **9**; factor 76 for **14** vs **10**). The initial results clearly showed that the 4-bromothenyl (4-BT) derivative **10** was the most active inhibitor ($IC_{50} = 0.009$ μM) and that its glucoside **14** ($IC_{50} = 2.0$ μM) was nearly as potent as the parent benzyl derivative **8** (O^6-BG). Therefore, in a second round of synthesis only the 4-BT guanine derivative was used for coupling to glucosides with various spacers, leading finally to the deprotected compounds **16**, **18**, **20**, **22**, **24**, and **26**.

The experimentally determined IC_{50} values for these additional compounds are also listed in Table 1. With the butyl or hexyl spacer (**16** or **18**), the IC_{50} is 0.45 μM. For longer spacers with $n = 8$, 10, 12 (compounds **20**, **22**, and **24**) there is a significant improvement in inhibition with IC_{50} = ca. 0.03 μM in each case. Finally, for the more rigid medium-sized but-2-ynyl spacer an intermediate IC_{50} of 0.25 μM was observed. Thus, essentially equal and maximum activities for glucosides were achieved with a flexible spacer of 8−12 methylene groups. While the IC_{50} values for compounds **20**, **22**, and **24** are still about a factor of 3 higher than for the parent guanine derivative **10**, the glucosides are expected to offer significant advantages in tumor selectivity, as described in the Introduction.

Molecular Modeling. To gain more insight into the experimentally observed structure−activity relationships, we constructed a 3D model of the MGMT-ligand complex using molecular dynamics (MD) simulations (including solvent water molecules) and docking experiments as described in the Methods. When we began these modeling experiments, only the coordinates of the crystal structure for O^6-alkylguanine-DNA methyltransferase were available (Protein Databank (PDB) entry 1QNT, resolution 1.90 Å, *R* value 0.198). These data served as a basis for MD simulations of MGMT complexes with 2-[O^6-(4-bromothenyl)-guan-9-yl]-ethyl-β-d-glucoside **(14)** and 8-[O^6-(4-bromothenyl)-guan-9-yl]-octyl-β-d-glucoside **(20).** During this work the crystal structures of the methyl and benzyl Cys145-thioether adducts of MGMT were published (PDB entries: 1EH7 (resolution 2.0 Å, R = 0.199) and 1EH8 (resolution 2.5 Å, R = 0.194), respectively).[30] To test our simulation results for the MGMT complex with **14**, we superimposed the backbones of the 1000 structures (snapshots) obtained during the MD run onto the crystal structure of *S*-benzyl MGMT. The RMS deviation for all backbone atoms was 0.79 ± 0.30 Å (mean ± SD), and the mean distance between the center of the benzyl ring in the covalently modified protein and the center of the 4-BT thiophene ring in our complexes was only 1.02 ± 0.33 Å (range: 0.29−1.71 Å). This correspondence between the modeled complex with **14** and the Cys145-benzylated enzyme is illustrated in Figure 1 for one of the MD-derived structures. Thus, the O^6 substituent of the tested ligand adopts a position within the binding pocket of MGMT which corresponds closely (but not exactly) to the position of the benzyl group attached covalently to Cys145 via reaction with O^6-BG. This finding was also confirmd by an MD simulation for the MGMT complex with ligand **20** (octyl spacer).

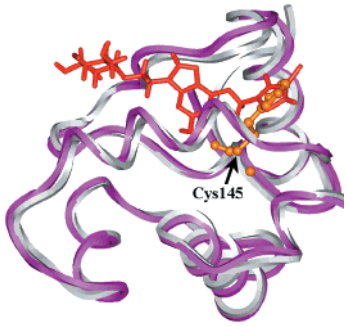

Figure 1. Superposition of the modeled structures of [*S*-benzyl Cys145]MGMT (from the crystal structure data, PDB entry: 1EH8, peptide C_α backbone = white/gray ribbon, *S*-benzyl group = brown ball-and stick model, arrow points to C_β) and the MGMT:**14** complex (magenta ribbon and red stick model). The complex represents a snapshot from a molecular dynamics simulation which included explicit water molecules and used the crystal structure of native MGMT (PDB entry: 1QNT) as a template.

The crystal structure of the *S*-benzylated MGMT product (PDB entry: 1EH8) reveals that Tyr158 and Asn137 flank the *S*-benzylcysteine side chain so closely that free rotation around either the cysteine or benzylic CH_2−S bond is not possible. A detailed interaction analysis for the MGMT:**20** complex was performed (see

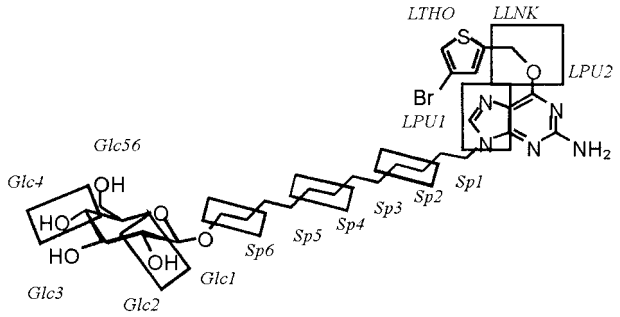

Figure 2. Definition of the structural subunits of MGMT inhibitors (example: compound **24**) for which enzyme:inhibitor interaction analysis was performed by molecular modeling. The subunits Sp1−Sp6 represent successive C_2 of the spacer, beginning at the guanyl N9 position.

Table 2. Local Interaction Energy Analysis for the Guanyl Fragment of Compound **20** in Its Complex with MGMT[a]

	guanyl region[b]				
residue	LTHO	LLNK	LPU1	LPU2	sum
Tyr 114			0.2	0.4	0.6
Gly 131			0.7	0.1	0.8
Met 134	0.5	0.8	0.5	0.9	2.6
Arg 135	1.2	0.9	1.2	0.6	3.9
Asn 137	1.1				1.1
Pro 140	1.1				1.1
Cys 145	0.2	0.3		0.7	1.2
Val 148				0.5	0.5
Asn 157			1.7	0.5	2.2
Tyr 158	1.5	1.4	1.6	1.5	6.0
Ser 159	1.0	1.0	0.5	0.5	2.9
Gly 160	0.7				0.7
sum	**7.2**	**4.4**	**6.3**	**5.8**	**23.7**

[a] Mean values for the local interaction energies (nonbonded van der Waals and Coulomb energies in kcal/mol) are *negative* and represent contributions to the stabilization of the MGMT:**20** complex, as determined from 1000 structures in the molecular dynamics archive. Results are rounded to one decimal place and values < 0.04 are not shown. [b] As defined in Figure 2.

Methods), whereby the local interaction energies between specific portions of the ligand molecule (as defined in Figure 2) and specific amino acid residues were calculated. The complete results of this study for seven 4-BT ligands are provided in the form of Supporting Information. Selected results for four regions of the guanyl portion of ligand **20** are summarized in Table 2, with negative nonbonded interaction energies representing a stabilization of the enzyme-ligand complex. The interaction of the O^6-substituent 4-BT (region LTHO) with the enzyme (−7.2 kcal/mol) represented about 30% of the total enzyme-guanyl stabilization energy (−23.7 kcal/mol). The strongest interactions involved Tyr158, Arg135, and Asn137 (−1.5, −1.2, −1.1 kcal/mol), consistent with the geometry of *S*-benzyl MGMT discussed above. Weaker interactions of the O^6 substituent of **20** were observed with Pro140, Ser159, and Gly160 (−1.1, −1.0, −0.7 kcal/mol), whose importance in the binding of O^6-BG (**8**) has been discussed in several publications.[31,33,36,44] The weaker interactions of **20** can be rationalized on the basis that in the complex the mean distances between the 4-BT group (center of ring) and the Cα of Pro140, Ser159, and Gly160 range from 5.7 to 5.9 Å and are 0.5−1.4 Å larger than the corresponding distances in *S*-benzyl MGMT.

The region of the ether linkage (LLNK) in **20** between the thiophene and the guanine moieties supplied about

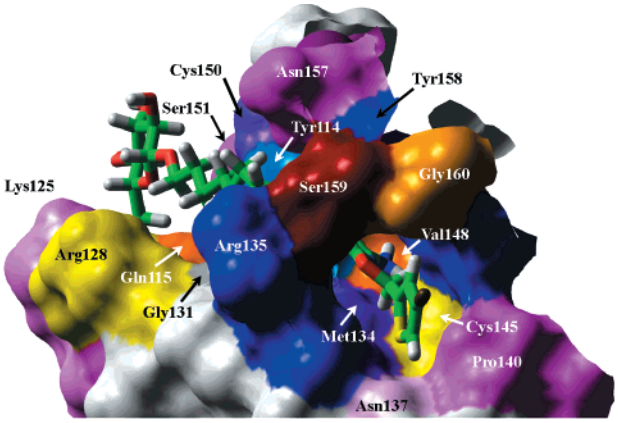

Figure 3. Snapshot taken from a molecular dynamics simulation of the MGMT:**20** complex (octyl spacer). The crystal structure of native MGMT (PDB entry: 1QNT) was used as a template. The inhibitor is represented as a stick model (green: C, white: H, red: O, blue: N, brown: Br, yellow: S). The water-accessible surface of the protein is shown using different colors for each amino acid residue. This view looks into the "tunnel" region, which interacts with the guanine moiety, and shows the O^6 substituent emerging in the foreground (lower right).

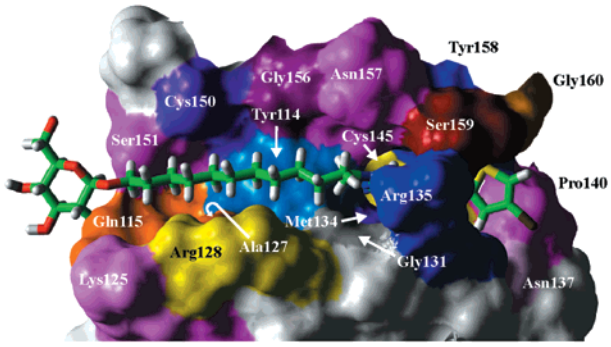

Figure 4. Snapshot taken from a molecular dynamics simulation of the MGMT:**24** complex (dodecyl spacer). The color coding is the same as in Figure 3, but here the complex has been rotated about 90° around a vertical axis to give a better view of the cleft into which the spacer region of the inhibitor fits. The glucose and guanine regions are, respectively, at the left and right ends of the inhibitor molecule.

19% of the total interaction energy and exhibited significant contacts with four of the residues that interacted with the thiophene itself, namely Met134, Arg135, Tyr158, and Ser159. The purine system (LPU1 + LPU2) generated about 51% of the interaction with MGMT, with about equal contributions coming from the five- and six-membered rings. The major interactions involved Met134, Arg135, Asn157, Tyr158, and Ser159 with minor contributions from Tyr114, Gly131, Asn137, Pro140, Cys145, Val148, and Gly160 (Table 2). As can be seen in Figures 3 and 4 several of these residues form a tunnel-like pocket in the active site of MGMT which can accommodate the guanyl portion of the ligand. At the end of the tunnel are the residues Asn137, Pro140, and Gly160 which interact only with the O^6 substituent. We find that the orientation of the guanyl portion of the ligand is very similar to that modeled by Wibley et al.[23,29] for the ligand O^6-BG. Therefore, we believe that our computational approach provides realistic models for MGMT complexes with our new ligands, such as **20** (Figure 3).

Table 3. Interaction Energy Analysis for Individual Amino Acid Residues in MGMT:Inhibitor Complexes[a]

	compound spacer													
	14 ethyl		16 butyl		18 hexyl		20 octyl		22 decyl		24 dodecyl		26 but-2-ynyl	
region	A	B	A	B	A	B	A	B	A	B	A	B	A	B
Ser 113									0.5	0.5	0.1	0.1		
Tyr 114	0.6	0.3	3.6	2.8	2.6	2.0	3.8	3.2	4.3	3.3	5.0	3.9	1.0	0.3
Gln 115			0.7	0.7	0.6	0.6	1.1	1.1	2.8	2.8	1.5	1.5		
Lys 125			0.1	0.1			0.5	0.5						
Ala 127			1.3	1.3	1.4	1.4	1.6	1.6	0.7	0.7	0.5	0.5	0.1	0.1
Arg 128	1.4	1.4	1.6	1.6	3.0	3.0	3.8	3.8	1.8	1.8	0.9	0.9	0.9	0.9
Gly 131	0.6	0.5	1.8	0.1	0.5	0.4	1.2	0.4	1.4	0.7	1.1	0.1	1.1	0.4
Gly 132	0.2	0.2	0.1						0.1				0.1	
Met 134	0.4		2.5		2.7		2.6		2.2		1.9		2.1	
Arg 135	4.7	2.6	3.0	0.1	2.3	0.6	3.9		2.1	0.1	2.8		2.2	0.6
Gly 136	0.1		0.1						1.5					
Asn 137	0.3		0.8		0.2		1.1		1.5		0.8		0.4	
Pro 138											0.2			
Val 139											0.1			
Pro 140	0.7		0.3		0.9		1.1		0.3		0.8		0.3	
Ile 141	0.2				0.6									
Cys 145	0.9		1.3		2.2		1.2		1.0		1.1		1.6	
His 146	0.6				1.4								1.2	
Val 148	0.2		0.4		0.4		0.5		0.4		0.2		0.9	
Val 149			0.1	0.1									0.1	
Cys 150			0.5	0.5					1.0	1.0	0.6	0.6		
Ser 151									0.9	0.9	0.4	0.4		
Ser 152									1.3	1.3	0.3	0.3		
Ala 154									0.2	0.2				
Val 155					1.2	1.1			1.7	1.7				
Asn 157	1.0	0.3	2.1	1.0	0.9	0.2	2.9	0.7	1.0	0.3	2.0	0.7	1.4	0.1
Tyr 158	5.4	0.4	6.4	0.4	6.8	0.5	6.0		5.6	0.3	5.7		3.9	
Ser 159	2.3		2.7		3.1		2.9		3.1		2.4		0.7	
Gly 160	0.7		0.5		1.0		0.7		1.5		1.2			
Gly 161	0.5		0.1		0.6									
Val 164	0.4				0.5								0.4	
Lys 165	0.1				0.1								0.2	
Leu 168					0.1								0.3	
sum	**21.5**	**5.8**	**30.0**	**8.5**	**33.1**	**9.7**	**34.9**	**11.3**	**37.2**	**15.8**	**29.7**	**9.1**	**19.1**	**2.5**

[a] Mean values for interaction energies (nonbonded van der Waals and Coulomb energies in kcal/mol) are *negative* and represent contributions to the stabilization of the MGMT:**20** complex, as determined from 1000 structures in the molecular dynamics archive; A = total interaction energy for complete ligand; B = interaction energy for glucosyl + spacer region only (N9 substituent). Only residues with total interactions (A) > 0.1 are shown; results are rounded to one decimal place and values <0.04 are not shown.

The favored orientation of the purine ring system determined by modeling directs the alkyl spacer at N9 along a cleft on the protein surface near helix 6. This is illustrated in Figure 4 for compound **24**. For the complete series of 4-BT ligands with various spacers, Table 3 summarizes the interaction energies between individual amino acid residues and the entire ligand (column A) or just the glucosyl+spacer region (N9 substituent) (column B). When the entries in columns (A) and (B) in Table 3 are nearly equal, then the corresponding amino acid residue interacts primarily with the N9 substituent rather than the guanyl portion of the ligand. This is the case for Tyr114, Gln115, Ala127, Arg128, Gly131, and Ser152, which have been identified to play an important role in the proposed nucleotide flipping mechanism required for DNA repair,[30] and also for Lys125, Cys150, Ser 151, and Val155. Thus, our model of the MGMT:inhibitor complex and the data of Table 3 reveal that our ligands can interact strongly with and therefore block residues normally involved in DNA binding.

The MD-derived interaction energies for MGMT:inhibitor complexes can also be viewed in terms of the local contributions made by each of the 15 structural elements of the ligand (Figure 2), summed across all amino acid residues involved, as shown in Table 4 for the 4-BTG glucosides **14, 16, 18, 20, 22, 24**, and **26**. In general, the interactions of the alkyl spacer and the glucose moiety with the face of the binding cleft are significantly weaker than the interactions of the "active" guanyl portion of the ligand in the binding "tunnel". For the inhibitor with the shortest ethyl spacer (**14**) or the more rigid butynyl spacer (**26**), the interaction energies for both the spacer and the glucose moiety are low. For these ligands the bulky glucose fits poorly into the binding cleft and prohibits an optimal fit of the guanyl portion, whose interaction energy is reduced to ca. 16 kcal/mol. With longer, more flexible spacers (butyl to dodecyl) the guanyl moiety can achieve its maximal stabilization in the binding pocket (21−23 kcal/mol), while the spacer itself can achieve up to 9 kcal/mol stabilization in the hydrophobic cleft. Maximum interaction with the N9 substituent is achieved with the decyl spacer (**22**). With the dodecyl spacer (**24**) the glucose moiety extends outside of the binding cleft and contributes little to the total binding interaction (Figure 4).

Figure 5 presents a correlation diagram for the calculated interaction energies (total, spacer+glucose, spacer alone) and the experimental IC_{50} values of the 4-BT glucoside inhibitors studied. While the data for the family of six inhibitors with $(CH_2)_n$ spacer show a crude negative correlation between the energies and IC_{50}, the data for the unique inhibitor **26** with butynyl spacer

Table 4. Total Interaction Energies for Specific Inhibitor Regions in MGMT:Inhibitor Complexes[a]

		compound (spacer)						
row	region	14 (ethyl)	16 (butyl)	18 (hexyl)	20 (octyl)	22 (decyl)	24 (dodecyl)	26 (but-2-ynyl))
1	LTHO	5.5	6.5	8.6	7.2	6.7	7.5	6.8
2	LLNK	2.3	3.9	3.6	4.4	3.9	3.7	2.5
3	LPU1	4.2	5.9	6.2	6.3	6.0	4.9	3.8
4	LPU2	3.8	5.1	5.0	5.8	4.8	4.5	3.5
∑ 1−4	**guanyl**	**15.7**	**21.5**	**23.4**	**23.7**	**21.3**	**20.6**	**16.6**
5	Sp1	2.0	1.7	2.1	1.5	2.1	1.2	0.7
6	Sp2		2.3	1.6	1.3	1.9	1.5	0.9
7	Sp3			1.9	2.0	2.3	1.6	
8	Sp4				1.6	1.9	1.1	
9	Sp5					0.9	1.1	
10	Sp6						1.1	
∑ 5−10	**spacer**	**2.0**	**4.0**	**5.6**	**6.4**	**9.0**	**7.4**	**1.6**
11	Glc1	0.8	0.8	1.1	2.0	2.5	0.6	0.3
12	Glc2	0.2	1.1	0.9	0.4	2.1	0.7	0.2
13	Glc3	0.3	0.3	0.4	0.2	1.1	0.0	0.0
14	Glc4	0.4	0.3	0.3	0.3	0.3	0.0	0.0
15	Glc56	2.1	2.0	1.5	2.0	0.8	0.4	0.5
∑ 11−15	**glucosyl**	**3.8**	**4.5**	**4.1**	**4.9**	**6.8**	**1.6**	**1.0**
∑ 1−15	**whole inhibitor**	**21.5**	**30.0**	**33.1**	**34.9**	**37.2**	**29.7**	**19.1**

[a] Energies are negative and in kcal/mol (see footnote in Table 3); structural regions are defined in Figure 2.

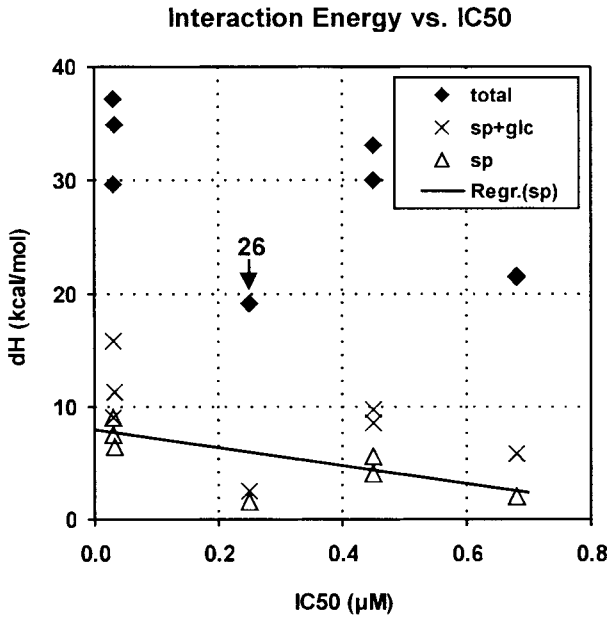

Figure 5. Correlation plot for MGMT:inhibitor interaction energies and IC_{50}. The vertical axis represents the calculated interaction energies (dH in kcal/mol) for the total ligand, the spacer+glucose subunit (sp+GLC), and the spacer alone (sp); the horizontal axis represents the IC_{50} values estimated from the in vitro assay (Table 1). Data points are shown for compounds **14**, **16**, **18**, **20**, **22**, and **24** and were analyzed by linear regression (solid line: spacer alone, $r^2 = 0.82$). Data points for the unique ligand (**26**) with butynyl spacer are marked with an arrow and were omitted from the analysis.

deviate significantly from the trend. Although the interaction energy for **26** is 11 kcal/mol less than for **16** (butyl spacer), the IC_{50} for **26** is actually about a factor of 2 lower than for **16**. This apparent conflict suggests that the modeling of the MGMT:**26** complex may be inadequate and deserves further study. For the inhibitors with $(CH_2)_n$ spacer a simple linear regression analysis indicates that the best correlation is obtained between IC_{50} and the interaction energy for the alkyl spacer alone (Figure 5, $r^2 = 0.82$). A poorer correlation ($r^2 = 0.54$) is observed for the spacer+glucose energy and for the total energy and may be due to the complex influence of spacer length on the interactions between protein and the glucosyl and guanyl subunits. However, due to the crudeness of the methods used for determining interaction energies and IC_{50} values and the relatively small differences observed, a more detailed quantitative analysis does not seem warranted at this time and would require the measurement of true binding constants and the calculation of free energies of binding (ΔG).

In summary, the modeling studies provide us with a simple rationale for interpreting the experimental MGMT inhibition assay results, at least on a qualitative basis. Glucosides **12**, **14**, and **28** with C_2 spacers are significantly poorer ligands compared to their parent guanines **8**, **9**, and **10**. The modeling experiments with **14** show that this can be explained by the poor fit of the glucosyl unit into the MGMT binding groove and the resulting nonoptimal binding geometry for the guanyl unit (lower interaction energy). With C_4 and C_6 spacers (**16**, **18**) a substantial improvement in interaction energy but only a modest improvement in inhibition was observed. The best inhibitors (**20**, **22**, and **24**) with spacers of 8−12 carbons exhibited the strongest protein−spacer interactions, and with the C_{10} spacer a maximum in protein−spacer and protein−glucose interaction was achieved. Elongation of the spacer from 10 to 12 carbons provided no improvement in inhibition and nearly eliminated binding stabilization via the glucosyl moiety. In addition, longer alkyl spacers, which are undesirable on the basis of solubility, can show diminishing returns due to the increased entropic penalty paid to form a complex with reduced degrees of rotational freedom. Thus, for more detailed quantitative structure−activity relationships it will also be important to consider the reduction in enthalpy required to orient the spacer and glucose unit in the appropriate conformation which provides a good "fit" to the surface of the protein and a maximum in stabilization energy. Finally, the MGMT:inhibitor model allows us to investigate local protein−spacer interactions in more detail and to design and test more structured spacers which may provide specific enhanced binding interactions.

Materials and Methods

MGMT Assay. The MGMT assay has been described previously.[45] Briefly, 200 μg of extracted cellular protein from HeLaS3 cells (ATCC, Rockville, MD) in 200 μL of 70 mM HEPES buffer (with 1 mM dithiothreitol (DTT), 5 mM EDTA, pH 7.8) was incubated at 37 °C with a defined concentration of MGMT inhibitor (added as a DMSO solution). After 30 min an excess of [^{3}H]-methylated DNA (120 000 cpm) was added, and the incubation was continued for an additional 90 min. The reaction was stopped by the addition of 400 μL TCA (13%), and the DNA was hydrolyzed by heating the reaction mixture for 30 min at 98 °C. The precipitated protein was washed three times with 400-μL portions of 5% TCA, solubilized in 0.1 N NaOH, and analyzed by liquid scintillation counting using the cocktail Rotiszint eco plus (Roth, Karlsruhe) and a TRI-CARB 2100 TR liquid scintillation analyzer (Canberra-Packard, Dreieich). Enzyme activity was expressed as fmol of [^{3}H]methyl transferred to TCA-insoluble protein material per mg of total cellular protein. Percent inhibition was calculated relative to untreated control samples. Each assay was repeated three times, and IC_{50} values were determined graphically from plots of percent inhibition vs inhibitor concentration.

Molecular Modeling. The crystal structure of the alkyltransferase MGMT (PDB entry: 1QNT, resolution 1.90 Å, *R* value 0.198) was used to derive a model for ligand binding in the active site. To reduce the required computational time for molecular dynamics, the amino acid residues 1−82 of the N-terminal region were deleted since these residues do not participate in the active site around Cys145 which is completely located within residues 83−176 of the C-terminal domain. Hydrogen atoms were added to the crystal structure assuming a pH of 7. The atom types and partial charges defined for the CFF91 force field were assigned using the automatic procedures of the modeling software INSIGHT II (Molecular Simulations, Inc., San Diego, CA). The ligand molecules were constructed manually using the BUILDER option of INSIGHT II. The guanine portion of the ligand molecules was initially docked by hand into the active site according to the orientation found for O^6-benzylguanine in previous modeling experiments by Wibley et al.[23,29]

The protein−ligand complex was placed in the center of a box (50 × 40 × 50 Å) which was filled with 2720 water molecules. The program DISCOVER (Molecular Simulations, Inc., San Diego, CA) was used to perform a molecular dynamics (MD) simulation with explicit solvent molecules under a standardized protocol for all complexes investigated. To ensure that the tertiary structure of the protein was maintained during the simulation, all backbone atoms of MGMT(83-176) were tethered to their original coordinates with a force constant of 100 kcal/Å, while side chains were unrestrained. The simulation protocol was defined as follows: integration step size = 1 fs, dielectric = 1.0, cutoff for nonbonded interactions = 10 Å, T = 300 K, periodic boundary conditions. In the initial phase an energy minimization of the complex was performed (1000 iterations). This was followed by a temperature equilibration period of 50 ps (velocity rescaling for ΔT > 10 K) and a production period of 1 μs with constant bath temperature maintained by the standard DISCOVER algorithm. During the production period, snapshots of the molecular ensemble were stored every 1000 steps (1 ps). This resulted in an archive of 1000 conformations which was used to produce trajectories for various structural parameters and to carry out the interaction analyses described in the Results. The ENCLOSE option of DISCOVER was used to calculate the nonbonded interactions (van der Waals and Coulombic) for specified structural elements of the ligand (Figure 2) with individual residues of MGMT. For each ligand fragment the calculation was performed for all residues for which at least one atom was within a radius of 5 Å measured from any atom of the ligand fragment. Water molecules were not included in the interaction calculation. All reported results represent average values for n = 1000 structures. These detailed analyses were carried out using software developed in the Central Spectroscopy Department by Martin Frank [Ph.D. Thesis: Conformational Analysis of Oligosaccharides in free and bound states; University of Heidelberg, (http://www.ub.uni-heidelberg.de/archiv/605/)]. The program PAVDO was used to extract relevant details from the large DISCOVER output files and to generate tables and lists which were used as input for the CAT software (conformational analysis tools; http://www.dkfz-heidelberg.de/spec/martin/cat2000). CAT was used to convert the raw data into the desired interaction matrices and to calculate the desired averages. Each MD simulation required ca. 7 days of computation with four parallel processors on an IBM SP2 computer.

Analytical Methods. HPLC separations were carried out on a Jasco HPLC system, consisting of a PU980 pump, a DG980-50 ternary gradient unit, a LG980-02 three-line degaser, and a UV975 intelligent UV−vis detector. Solvents were of the highest purity available; water was degassed under vacuum, other solvents by ultrasound. A variety of HPLC methods and solvent gradients were employed and are designated here by roman numerals (see Table B, Supporting Information). For methods I, III, IV, VI, VII, VIII, X, and XII a Lichrospher column (100-RP18-(E)-5 μm; 250 × 4 mm) and methanol/water at a flow rate of 1 mL/min were used with UV detection at 254 nm. Methods II and XI utilized a Lichrospher column (100-RP18-(E)-5 μm; 250 × 4 mm), acetonitrile/water at a flow rate of 1 mL/min, and UV detection at 254 nm. For methods V and IX the setup was as follows: Purospher column (Si80−5 μm; 250 × 4.6 mm), chloroform/methanol at 1 mL/min, UV detection at 254 nm. TLC analysis was performed with solvents of the highest purity available, and mixtures are reported in %(vol/vol). Precoated plastic sheets were from Macherey-Nagel, Type Polygram SIL G/UV_{254}. Column and flash chromatography were carried out with silica gel from Macherey-Nagel, Type Silica Gel 60, either 70−230 mesh ASTM (column chromatography) or 230−400 mesh ASTM (flash chromatography).

Mass spectrometry was performed with a Finnigan MAT TSQ-7000 using electrospray ionization (ESI) or with a JEOL JMS 700 in high-resolution mode using fast-atom bombardment (HR−FAB). Uncorrected melting points were determined with a Büchi apparatus. UV spectra were recorded with a Hitachi Uvikon 931 spectrophotometer.

^{1}H- and ^{13}C NMR spectra were recorded using Bruker NMR spectrometers: AC-250 (5.87 T, 250 MHz ^{1}H frequency) and AM-500 (11.74 T, 500 MHz ^{1}H frequency), with 5-mm sample tubes and standard Fourier transform NMR techniques. In general, the protected glucosides were dissolved in $CDCl_3$ and measured at 30 °C at 5.87 T (data reported in text below), while the deprotected glucosides (final products) were measured at 37 °C or 40 °C in DMSO-d_6 at 11.74 T (detailed data are reported in Tables D−G, Supporting Information). For all compounds one-dimensional ^{1}H and ^{13}C (^{1}H-decoupled and DEPT) spectra were obtained. In general, a complete first-order ^{1}H spin system analysis was performed with Bruker's WIN NMR software using zero filling and resolution enhancement (Lorentz-Gauss line shape transformation). For compounds **10**, **14**, **19**, and **20** additional experiments were performed at 11.74 T: 2D HH−COSY, 2D CH correlation via $^1J_{CH}$ or via $^nJ_{CH}$ (COLOC, compound **19**), 1D ^{13}C with gated and selective ^{1}H decoupling to observe and assign J_{CH} for nonprotonated carbons. Detailed measurements were also made for **10** and **20** in $CDCl_3$/CD_3OD at 30 °C and for the butyl spacer analogue (not used in this study) of the 8-aza compound **28** in DMSO. Thus, for these compounds complete and unequivocal signal assignments could be made a priori. These results, other literature data, and chemical shift predictions using SpecTool software (version 2.1, Chemical Concepts, Weinheim, FRG) and WIN−SPECEDIT (version 3.0, Bruker) served as a basis for all other assignments reported here. The few remaining ambiguities are duly noted in the results. ^{1}H chemical shifts are reported in ppm relative to the following internal references: tetramethylsilane (TMS) in $CDCl_3$ = 0.0, residual DMSO-d_5 = 2.49 ppm, residual CHD_2OD = 3.30; ^{13}C chemical shifts are relative to $CDCl_3$ = 77.0, DMSO = 39.5, or CD_3OD = 49.0 ppm. Spin−spin J couplings are reported in

Hz. For signal assignments the numbering scheme shown in Chart 1 is used, and the alkyl spacer is numbered beginning at the glucoside $-OCH_2$.

Syntheses. Synthesis of Activated Alkyl Glucosides (1−7). The Königs-Knorr method (Chart 2, step A) was used to prepare the required ω-bromoalkyl-β-d-glucopyranosides, as described below.[46] Detailed NMR data with assignments are presented below only for the representative compounds **1**, **4**, and **7** (ethyl, octyl, butynyl spacer); the corresponding data for compounds **2**, **3**, **5**, and **6** are provided as Supporting Information. The specific ^{13}C NMR assignments given are generally unambiguous with the exception of Glc2, Glc5 (assigned by analogy with **19**) and the inner carbons of long alkyl chains (Alk4 to Alk(ω-3), which were assigned by analogy with **19** and by considering shift increment rules for alkanes.

2-Bromoethyltetra-*O*-acetyl-β-d-glucopyranoside (1). 2-Bromoethanol (12.5 g, 100 mmol) and 9.85 g (20 mmol) of 1,2,3,4,6-penta-*O*-acetyl-β-d-glucopyranoside were dissolved in 50 mL of dry methylene chloride and stirred with 4-Å molecular sieves for 1 h under argon. After addition of 5.4 mL (30 mmol) of trimethylsilyltriflate stirring was continued until no glucose educt could be detected by TLC. The reaction was stopped by addition of 3.3 g (30 mmol) of triethylamine, and the pH was adjusted to 6−7 with solid sodium carbonate. The mixture was filtered, and the filtrate was shaken with four 80-mL portions of saturated sodium carbonate solution. The organic phase was dried over sodium sulfate. After evaporation of the solvents the product was separated by flash chromatography on SiO_2 (7.5 × 25 cm) with ethyl acetate/petroleum ether (1:2) to yield pure **1** (4.1 g, 36.1%). Recrystallization was achieved by adding water to a methanol solution of the product; cooling to 4 °C gave analytically pure white needles. $C_{16}H_{23}BrO_{10}$ (M_r = 455.05); TLC: R_f 0.49 (SiO_2, petroleum ether/ethyl acetate 1:1); ESI-MS: *m*/*z* (% int.) 477.1/479.1 (98/100) $[M(^{79}Br/^{81}Br) + Na]^+$ (calc. 477.04/479.03).

^1H NMR δ_H (250 MHz, CD_3OD): 1.960; 1.999; 2.027; 2.049 (4 s, acetyl CH_3); 3.474 (ddd, Alk2b), 3.542 (ddd, Alk2a); 3.855 (ddd, Alk1b); 3.872 (ddd, Glc5); 4.102 (ddd, Alk1a); 4.134 (dd, Glc6b); 4.271 (dd, Glc6a); 4.731 (d, Glc1); 4.898 (dd, Glc2); 5.014 (dd, Glc4); 5.254 (dd, Glc3). ^1H *J* couplings (Hz): 7.95 (Glc1,2); 9.50 (Glc2,3); 9.43 (Glc3,4); 10.0 (Glc4,5); 4.67 (Glc5,6a), 2.48 (Glc5,6b); −12.35 (Glc6a,6b); −11.54 (Alk1a,1b); 5.40 (Alk1a,-2a); 5.55 (Alk1a,2b); 5.43 (Alk1b,2a); 7.30 (Alk1b,2b); −10.70 (Alk2a,2b).

^{13}C NMR δ_C (62.9 MHz, CD_3OD): 20.53; 20.55; 20.62; 20.74 (4, acetyl CH_3); 31.17 (Alk2); 63.07 (Glc6); 69.83 (Alk1); 71.01 (Glc4); 72.68 (Glc2); 72.91 (Glc5); 74.17 (Glc3); 101.83 (Glc1); 171.15; 171.22; 171.58; 172.27 (4 C═O).

4-Bromobutyltetra-*O*-acetyl-β-d-glucopyranoside (2). For this particular case only, the method of Helferich and Zirner[47] was used as published to produce **2** (1.2 g, 10%). $C_{18}H_{27}BrO_{10}$ (483.31); TLC: R_f 0.39 (SiO_2, petroleum ether/ethyl acetate 1:1); ESI-MS: *m*/*z* (% int.) 505.0/507.0 (42) $[M(^{79}Br/^{81}Br) + Na]^+$ (calc. 505.07/507.07), 987.3/989.2 (45/100) $[2M(^{79}Br/^{81}Br) + Na]^+$.

6-Bromohexyltetra-*O*-benzoyl-β-d-glucopyranoside (3). After 25 mL of nitromethane was dried for 20 h with 3-Å molecular sieves under argon, 5.5 g (30 mmol) of 1-bromo-6-hexanol and 3.3 g (5 mmol) of 1-bromo-2,3,4,6-tetra-*O*-benzoyl-β-d-glucopyranoside were added, and the reaction mixture was stirred for 60 min. After addition of 0.7 g of silver phosphate, the reaction was monitored by TLC until no glucose educt could be detected. After addition of 75 mL of ethyl acetate, the mixture was filtered, and the solvent was evaporated. Purification by flash chromatography on SiO_2 (5.5 × 20 cm) with petroleum ether/ethyl acetate (4:1) gave **3** as a colorless oil (2.2 g, 58%). $C_{40}H_{39}BrO_{10}$ (759.65); TLC: R_f 0.25 (SiO_2, petroleum ether/ethyl acetate, 4:1, developed twice); R_f 0.53 (SiO_2, petroleum ether/ethyl acetate 2:1); ESI-MS: *m*/*z* (% int.) 579.1 (100) $[M + H - Br(CH_2)_6OH]^+$, 759.2/761.2 (5) $[M(^{79}Br/^{81}Br) + H]^+$ (calc. 759.18/761.18), 781.1/783.1 (20) $[M(^{79}Br/^{81}Br) + Na]^+$.

8-Bromooctyltetra-*O*-benzoyl-β-d-glucopyranoside (4). As described for **3**, 1.22 g (5.8 mmol) of 1-bromo-8-octanol and 3.3 g (5 mmol) of 1-bromo-2,3,4,6-tetra-*O*-benzoyl-β-d-glucopyranoside were reacted. Flash chromatography on SiO_2 (4 × 20 cm) with petroleum ether/ethyl acetate (4:1) gave **4** as a colorless oil (1.92 g, 48%). $C_{42}H_{43}BrO_{10}$ (787.70); TLC: R_f 0.26 (SiO_2, petroleum ether/ethyl acetate, 4:1); ESI-MS: *m*/*z* (% int.) 579.1 (100) $[M + H-Br(CH_2)_8OH]^+$, 787.1/789.2 (5) $[M(^{79}Br/^{81}Br) + H]^+$ (calc. 787.21/789.21), 809.1/811.1 (30) $[M(^{79}Br/^{81}Br) + Na]^+$.

^1H NMR δ_H (250 MHz, $CDCl_3$): 1.1−1.30 (8H, Alk3,4,5,6); 1.48 (m, Alk2b); 1.56 (m, Alk2a); 1.719 (tt, Alk7); 3.313 (t, Alk8); 3.544 (dt, Alk1b); 3.924 (dt, Alk1a); 4.186 (ddd, Glc5); 4.529 (dd, Glc6b); 4.661 (dd, Glc6a); 4.865 (d, Glc1); 5.551 (dd, Glc2); 5.703 (dd, Glc4); 5.940 (dd, Glc3); 7.24−7.38 (m, 4 Bz3,5); 7.4−7.52 (m, 4 Bz4); 7.83−8.02 (m, 4 Bz2,6). ^1H *J* couplings: 7.83 (Glc1,2); 9.72 (Glc2,3); 9.62 (Glc3,4); 9.76 (Glc4,5); 3.35 (Glc5,6a); 5.05 (Glc5,6b); −12.09 (Glc6a,6b); −9.69 (Alk1a,1b); 6.14 (Alk1a,2); 6.6 (Alk1b,2); 6.87 (Alk7,8).

^{13}C NMR δ_C (62.9 MHz, $CDCl_3$): 25.54 (Alk3); 27.83 (Alk6); 28.38 (Alk4); 28.82 (Alk5); 29.20 (Alk2); 32.60 (Alk7); 33.76 (Alk8); 63.13 (Glc6); 69.79 (Glc4); 70.08 (Alk1); 71.86 (Glc2); 72.05 (Glc5); 72.87 (Glc3); 101.18 (Glc1); 128.14, 128.21, 128.21, 128.25 (4 Bz3,5); 128.72, 128.73, 129.28, 129.52 (4 Bz1); 129.6 129.6 129.6 129.67 (4 Bt2,6); 132.96, 133.05, 133.06, 133.26 (4 Bz4); 164.90, 165.07; 165.68; 165.97 (4 C═O).

10-Bromodecyltetra-*O*-benzoyl-β-d-glucopyranoside (5). As described for **3**, 1 g (4.3 mmol) of 1-bromo-10-decanol and 3.3 g (5 mmol) of 1-bromo-2,3,4,6-tetra-*O*-benzoyl-β-d-glucopyranoside were reacted. Flash chromatography on SiO_2 (4 × 20 cm) with petroleum ether/ethyl acetate yielded pure **5** as an colorless oil (1.62 g, 46%). $C_{44}H_{47}BrO_{10}$ (815.76); TLC: R_f 0.34 (SiO_2, petroleum ether/ethyl acetate 6:1, developed twice); ESI-MS: *m*/*z* (% int.) 579.1 (100) $[M + H - Br(CH_2)_{10}OH]^+$, 815.2/817.2 (5) $[M(^{79}Br/^{81}Br) + H]^+$ (calc. 815.24/817.24), 837.2/839.2 (92/100) $[M(^{79}Br/^{81}Br) + Na]^+$.

12-Bromododecyltetra-*O*-benzoyl-β-d-glucopyranoside (6). As described for **3**, 1 g (3.7 mmol) of 1-bromo-12-dodecanol and 2.5 g (3.7 mmol) of 1-bromo-2,3,4,6-tetra-*O*-benzoyl-β-d-glucopyranoside were reacted. Flash chromatography on SiO_2 (4 × 20 cm) with petroleum ether/ethyl acetate (4:1) gave pure **6** as an colorless oil (1.95 g, 62%). $C_{46}H_{51}BrO_{10}$ (843.81); TLC: R_f 0.34 (SiO_2, petroleum ether/ethyl acetate 6:1, developed twice); ESI-MS: *m*/*z* (% int.) 579.0 (95) $[M + H - Br(CH_2)_{12}OH]^+$, 843.1/845.1 (3) $[M(^{79}Br/^{81}Br) + H]^+$ (calc. 843.27/845.27), 865.2/867.1 (84/100) $[M(^{79}Br/^{81}Br) + Na]^+$.

4-Bromobut-2-ynyltetra-*O*-acetyl-β-d-glucopyranoside (7). In 5 mL of dry 1,2-dichloroethane were dissolved and stirred with 4-Å molecular sieves for 1 h under argon 745 mg (5 mmol) of 4-bromobut-2-yn-1-ol and 780 mg (2 mmol) of 1,2,3,4,6-penta-*O*-acetyl-β-d-glucopyranoside. After addition of 352 μL (2 mmol) of trimethylsilyltriflate, stirring was continued until no glucose educt could be detected by TLC. The reaction was stopped by addition of 218 mg (2 mmol) of triethylamine, and the pH was adjusted to 6−7 with solid sodium carbonate. The mixture was filtered, and 25 mL of chloroform was added to the filtrate, which was then shaken with four 25-mL portions of saturated sodium carbonate solution. The organic phase was dried with sodium sulfate. After evaporation of the solvents flash chromatography on SiO_2 (5.5 × 20 cm) with petroleum ether/ethyl acetate (1:1) gave the product **7** (160 mg, 16.7%). An analytically pure sample was obtained by recrystallization from methanol at −30 °C. $C_{18}H_{23}BrO_{10}$ (479.28); TLC: R_f 0.37 (SiO_2, petroleum ether/ethyl acetate 1:1); R_f 0.11 (SiO_2, petroleum ether/ethyl acetate 2:1); ESI-MS: *m*/*z* (% int.) 496.3/498.1 (30) $[M(^{79}Br/^{81}Br) + NH_4]^+$, 501.1/503.2 (92/100) $[M(^{79}Br/^{81}Br) + Na]^+$ (calc. 501.04/503.03).

^1H NMR δ_H (250 MHz, $CDCl_3$): 2.01, 2.03, 2.07, 2.09 (4 s, acetyl CH_3); 3.73 (ddd, Glc5); 3.94 (t, 2H, Alk4), 4.16 (dd, Glc6b); 4.27 (dd, G6a); 4.42 (t, 2H, Alk1); 4.73 (d, Glc1); 5.00 (dd, Glc2); 5.10 (dd, Glc4); 5.24 (dd, Glc3). ^1H *J* couplings: 7.8 (Glc1,2); 9.3 (Glc2,3); 9.3 (Glc3,4); 9.4 (Glc4,5); 4.5 (Glc5,6a); 2.3 (Glc5,6b); −12.3 (Glc6a,6b); 1.9 (Alk1,4).

^{13}C NMR (62.9 MHz): 13.70 (Alk4); 20.54, 20.56, 20.67, 20.67 (4 acetyl CH_3); 56.19 (Alk1); 61.75 (Glc6); 68.30 (Glc4); 71.01 (Glc2); 71.96 (Glc5); 72.78 (Glc3); 81.19, 82.34 (Alk2,3 assignments not definitive); 98.31 (Glc1); 169.34, 169.37, 170.21, 170.59 (4 C═O).

Synthesis of Guanine Derivatives (8−10). The required *O*⁶-*R* guanine derivatives were prepared as described in the Results and outlined below.

***O*⁶-Benzylguanine (8).** In 20 mL of benzyl alcohol was carefully dissolved 0.6 g (26 mmol) of sodium hydride, and the solution was heated to 130 °C. In small portions 2 g (11.8 mmol) of 2-amino-6-chloropurine was added, and the reaction mixture was stirred for 18 h, then cooled to room temperature, and neutralized with acetic acid. The benzyl alcohol was removed by distillation. Purification by column chromatography (SiO_2, dichloromethane/methanol, 20:1), yielded the product **8** (0.91 g, 31%). $C_{12}H_{11}N_5O$ (241.25); TLC: R_f 0.31 (SiO_2, dichloromethane/methanol 10:1); ESI-MS: *m*/*z* (% int.) 241.8 (100) $[M + H]^+$ (calc. 242.10), 263.8 (5) $[M + Na]^+$, 483.2 (15) $[2M + H]^+$.

^{1}H NMR δ_H (250 MHz, CD_3OD): 5.52 (s, 2H, Bn7); 7.30 (m, 1H, Bn4); 7.34 (m, 2H, Bn3,5); 7.48 (m, 2H, Bn2,6); 7.822 (s, 1H, G8). Aromatic protons were assigned by analogy with **12**.

^{13}C NMR δ_C (62.9 MHz, CD_3OD): 68.97 (T, Bn7); 113.37 (br S, G5); 129.11 (S, Bn4); 129.37 (D, Bn3,5); 129.45 (D, Bn2,6); 137.93 (S, Bn1); 140.04 (D, G8); 157.09 (br S, G4); 161.43 (S, G6); 161.70 (S, G2). Tautomerization between N9−H and N7−H leads to significant linebroadening (ca. 20 Hz) at G4,G5. Bn2,6 and Bn3,5 assigned by analogy with **12**.

8-Aza-*O*⁶-benzylguanine (9). In a mixture of 200 mL of acetone and 20 mL of acetic acid was suspended and stirred for 2 h 4.9 g (20 mmol) of 2,4,5-triamino-6-benzyloxypyrimidine and 1.38 g (20 mmol) sodium nitrite. The acetone was reduced in volume, and the mixture was shaken with 100 mL of water and 5 × 100 mL of chloroform to extract the product. Purification was performed via flash chromatography (SiO_2; chloroform/methanol 15:1), and **9** was crystallized from ethanol/water 1:1 (3.05 g, 63%). $C_{11}H_{10}N_6O$ (242.24); TLC: R_f 0.40 (SiO_2, dichloromethane/methanol 10:1); ESI-MS: *m*/*z* (% int.) 243.0 (50) $[M+H]^+$ (calc. 243.09), 264.9 (20) $[M + Na]^+$, 485.2 (80) $[2M + H]^+$, 507.1 (50) $[2M + Na]^+$.

^{1}H NMR δ_H (250 MHz, CD_3OD): 5.6 (s, Bn7); 7.32 (m, Bn4); 7.37 (m, Bn3,5); 7.52 (m, 2H, Bn2,6).

^{13}C NMR δ_C (62.9 MHz, CD_3OD): 69.74 (Bn7); 121.30 (G5); 129.38 (Bn4); 129.56 (Bn2,6; Bn3,5); 137.26 (Bn1); 156.13 (G4); 162.62 (G6); 164.06 (G2).

4-Bromothenyl Alcohol. In 400 mL of 2-propanol were stirred for 1 h 25 g (130 mmol) of 4-bromothiophen-2-aldehyde and 5.7 g (150 mmol) of sodium borohydride. The reaction was stopped by addition of 10 mL of water. The crude product was obtained by filtration and extracted with *n*-hexane (22.5 g, 89%). C_5H_5BrOS (193.06); TLC: R_f 0.38 (SiO_2, toluol/methanol 4:1); ESI-MS: *m*/*z* (% int.) 190.7/192.7 (40) $[M(^{79}Br/^{81}Br) - H]^-$ (calc. 190.92/192.92).

^{1}H NMR δ_H (250 MHz, $CDCl_3$): 2.539 (t, BT6-OH); 4.731 (dd, BT6); 6.887 (dt, BT3); 7.155 (d, BT5); $^3J_{6,OH} = 5.8$; $^4J_{3,5} = 1.44$; $^4J_{3,6} = 0.8$.

^{13}C NMR δ_C (62.9 MHz, $CDCl_3$): 59.38 (T, BT6); 109.27 (S, BT4); 122.31 (D, BT5); 127.43 (D, BT3); 145.88 (S, BT2).

***O*⁶-(4-Bromothenyl)guanine (10).** In 12 mL of DMSO was dissolved 13.89 g (72 mmol) of 4-bromothenyl alcohol, and the mixture was carefully treated with 1.92 g [48 mmol] of sodium hydride with stirring for 1 h. Then 5.49 g (24 mmol) of 2-aminopurin-6-yltrimethylammonium chloride was added in small portions, and the mixture was stirred for 1 h. The mixture was neutralized with 3.9 mL of acetic acid, followed by addition of 240 mL of diethyl ether, and stirred for 1.5 h. The solid material was dried and washed with water, and **10** was recrystallized from methanol at −15 °C (5.5 g, 70%). $C_{10}H_8BrN_5OS$ (326.17); TLC: R_f 0.4 (SiO_2, dichloromethane/methanol 10:1); R_f 0.22 (SiO_2, toluol/methanol 4:1); mp 212−214 °C; ESI-MS: *m*/*z* (% int.) 325.8/327.8 (98/100) $[M(^{79}Br/^{81}Br) + H]^+$ (calc. 325.971/327.969), 347.8/349.8 (19/20) $[M(^{79}Br/^{81}Br) + Na]^+$; λ_{max} (methanol) = 239, 284 nm.

^{1}H NMR δ_H (500 MHz, DMSO-d_6): 5.627 (d, BT6); 6.247 (s, br, 2-NH_2); 7.308 (dt, BT3); 7.650 (d, BT5); 7.820 (s, H8); 12.4 (br, N9−H). ^{1}H *J* couplings: 1.52 (BT3,BT5); 0.57 (BT3,BT6).

^{13}C NMR δ_C (125 MHz, DMSO-d_6): 60.47 (T, BT6); 107.88 (S, BT4); 112.75 (S,vbr, G5); 124.90 (D, BT5); 130.53 (D, BT3); 138.35 (D,br G8); 140.62 (S, BT2), 155.99 (s,vbr, G4); 158.73 (S,br, G6); 159.27 (S, G2). All guanine signals except G2 were broad (br) or very broad (vbr) due to tautomerization between N7H and N9H forms.

Synthesis of Protected Nucleoside Analogues (11, 13, 15, 17, 19, 21, 23, 25, and 27). The bromoalkyl glucosides were coupled with guanine derivatives via the following standard procedure (Chart 2, step B). One equivalent of the purine and 1 equiv of the activated alkylglucoside were dried for 12 h at 1×10^{-3} mmHg. The guanine derivatives were dissolved in very dry DMF (10 mL/mmol) containing 4-Å molecular sieves. Subsequently 1.1 equiv of lithium hydride was added, and the mixture was stirred for 1 h while increasing the temperature to 80 °C. The glycoside was dissolved in dry DMF (5 mL/mmol) and added dropwise to the solution of the guanine. Stirring was continued until one of the educts could no longer be detected by TLC. The reaction mixture was cooled to room temperature, 0.1 M phosphate buffer (KH_2PO_4/Na_2PO_4, pH 7) was added (10 mL/mmol), and the mixture was stirred for 15 min and then filtered. The filtrate was extracted with three 100-mL portions of chloroform. The organic phase was dried over sodium sulfate and evaporated until no DMF was left in the oily mixture. Purification of the product was achieved by column or flash chromatography (see below). The HPLC methods used are summarized in the footnote to Table B (Supporting Information). With the exception of **23**, where the reaction mixture was used directly for step C, all compounds were characterized by ^{1}H and ^{13}C NMR at 5.87 T (11.74 T for **19**). For the representative compounds **13**, **19**, **25**, and **27**, only the key NMR data required for characterization are presented below; the complete data for all compounds are provided as Supporting Information.

2-(*O*⁶-Benzylguan-9-yl)ethyl-*β*-d-tetra-*O*-acetylglucoside (11). The coupling reaction was carried out with 241 mg (1 mmol) of *O*⁶-benzylguanine and 455 mg (1 mmol) of 2-bromoethyl-tetra-*O*-acetyl-*β*-d-glucopyranoside. Column chromatography (3 × 15 cm) with ethyl acetate/petroleum ether (2:1) gave pure **11** (73.6 mg, 17.7%). $C_{28}H_{33}N_5O_{11}$ (615.60); TLC: R_f 0.5 (SiO_2, methylene chloride/methanol 20:1); HPLC (method II): R_t = 13.8 min; ESI-MS: *m*/*z* (% int.) 616.2 (100) $[M + H]^+$ (calc. 616.22), 638.2 (55) $[M + Na]^+$.

2-[*O*⁶-(4-Bromothenyl)guan-9-yl]ethyl-*β*-d-tetra-*O*-acetylglucoside (13). The coupling reaction was carried out with 163 mg (0.5 mmol) of *O*⁶-(4-bromothenyl)guanine and 225 mg (0.5 mmol) of 1-(2-bromoethyl)-2,3,4,6-tetra-*O*-acetyl-*β*-d-glucopyranoside. Column chromatography (1 × 20 cm) with acetone/petroleum ether (1:1) gave pure **13** (30 mg, 8.5%). $C_{26}H_{30}BrN_5O_{11}S$ (700.52); TLC: R_f 0.17 (SiO_2, acetone/petroleum ether 1:1); HPLC (method II): R_t = 13.9 min; ESI-MS: *m*/*z* (% int.) 700.1/702.1 (21/23) $[M(^{79}Br/^{81}Br) + H]^+$ (calc. 700.09/702.09), 722.1/723.9 (21/23) $[M(^{79}Br/^{81}Br) + Na]^+$, 1399.4/1401.3 (40/100) $[2M(^{79}Br/^{81}Br) + H]^+$.

^{1}H NMR δ_H (250 MHz, $CDCl_3$), selected data: 3.775 (ddd, Alk1b); 4.17 (m, Alk2b); 4.19 (ddd, Alk1a); 4.319 (ddd, Alk2a); 4.431 (d, Glc1); 4.863 (br s, 2H, G2-NH_2); 5.634 (d, BT6b); 5.663 (d, BT6a); 7.110 (dt, BT3); 7.182 (d, BT5); 7.582 (s, G8). ^{1}H *J* couplings: 7.84 (Glc1,2); −10.5 (Alk1a,1b); −14.7 (Alk2a,2b); 1.47 (BT3,5); 0.68 (BT3,6); −12.7 (BT6a,b).

^{13} C NMR δ_C (62.9 MHz, $CDCl_3$), selected data: 43.06 (Alk2); *61.74* (BT6); 67.45 (Alk1); 100.53 (Glc1); 109.13 (BT4); 115.32 (G5); 124.02 (BT5); 130.85 (BT3); 139.88 (BT2); 140.62 (G8); 154.19 (G4); 158.81 (G2); 160.20 (G6).

4-[*O*⁶-(4-Bromothenyl)guan-9-yl]butyl-*β*-d-tetra-*O*-acetylglucoside (15). The reaction was carried out with 163 mg (0.5 mmol) of *O*⁶-(4-bromothenyl)guanine and 241 mg (0.5 mmol) of 4-bromobutyltetra-*O*-acetyl-*β*-d-glucopyranoside. Column cromatography (3 × 25 cm) with acetone/petroleum ether (1:1) gave pure **15** (86 mg, 24.8%). $C_{28}H_{34}BrN_5O_{11}S$ (728.58); TLC: R_f 0.17 (SiO_2, acetone/petroleum ether 1:1); HPLC

(method II): R_t = 14.8 min; ESI-MS: *m/z* (% int.) 727.9/729.8 (90/100) $[M(^{79}Br/^{81}Br) + H]^+$ (calc. 728.12/730.12), 749.9/751.9 (90/85) $[M(^{79}Br/^{81}Br) + Na]^+$.

6-[*O*^{6}-(4-Bromothenyl)guan-9-yl]hexyl-*β*-d-tetra-*O*-benzoylglucoside (17). The reaction was carried out with 163 mg (0.5 mmol) of *O*^{6}-(4-bromothenyl)guanine and 378 mg (0.5 mmol) of 6-bromohexyltetra-*O*-benzoyl-*β*-d-glucopyranoside. Flash chromatography (3.5 × 30 cm) with petroleum ether/acetone (1:1) gave pure **17** (150 mg, 29.8%). $C_{50}H_{46}BrN_5O_{11}S$ (1004.91); TLC: R_f 0.31 (SiO_2, acetone/petroleum ether 1:1); R_f 0.23 (SiO_2, ethyl acetate/petroleum ether 2:1); HPLC (method II): R_t = 20.8 min; ESI-MS: *m/z* (% int.) 1004.0/1006.3 (100/75) $[M(^{79}Br/^{81}Br) + H]^+$ (calc. 1004.22/1006.22), 1025.9/1027.9 (17/13) $[M(^{79}Br/^{81}Br) + Na]^+$.

8-[*O*^{6}-(4-Bromothenyl)guan-9-yl]octyl-*β*-d-tetra-*O*-benzoylglucoside (19). The reaction was carried out with 0.82 g (2.5 mmol) of *O*^{6}-(4-bromothenyl)guanine and 1.82 g (2.5 mmol) of 8-bromooctyltetra-*O*-benzoyl-*β*-d-glucopyranoside. Flash chromatography (4.5 × 25 cm) with petroleum ether/acetone (3:1) gave pure **19** (1.00 g, 37.7%). $C_{52}H_{50}O_{11}BrN_5S$ (1032.97); TLC: R_f 0.50 (SiO_2, acetone/petroleum ether 1:1); ESI-MS: *m/z* (% int.) 1032.5/1034.5 (85/100) $[M(^{79}Br/^{81}Br)+H]^+$ (calc. 1032.25/1034.25), 1054.5/1056.4 (15/18) $[M(^{79}Br/^{81}Br) + Na]^+$.

^{1}H NMR (500 MHz, $CDCl_3$, selected data): 3.523 (dt, Alk1b); 3.904 (dt, Alk1a); 3.971 (t, 2H, Alk8); 4.831 (d, Glc1); 4.964 (br, 2H, G2-NH_2); 5.643 (d, 2H, BT6); 7.111 (dt, BT3); 7.178 (d, BT5); 7.582 (s, G8). ^{1}H *J* couplings: 7.84 (Glc1,2); −9.7 (Alk1a,b); 7.3 (Alk7,8).

^{13}C NMR δ_C (125 MHz, $CDCl_3$, selected data): 25.64 (Alk3); 26.39 (Alk6); 28.76 (Alk5); 28.92 (Alk4); 29.30 (Alk2); 29.74 (Alk7); 43.60 (Alk8); 61.79 (BT6); 70.23 (Alk1); 101.34 (Glc1); 109.15 (BT4); 115.36 (G5); 124.06 (BT5); 130.84 (BT3); 139.72 (G8); 139.85 (BT2); 154.16 (G4); 158.78 (G2); 160.22 (G6). Selected ^{13}C−^{1}H couplings for carbon: G8 (209.2 d, 4.0 t); BT3 (174.2 d); BT5 (190.9 d, 8.1 d).

10-[*O*^{6}-(4-Bromothenyl)guan-9-yl]decyl-*β*-d-tetra-*O*-benzoylglucoside (21). The reaction was carried out with 163 mg (0.5 mmol) of *O*^{6}-(4-bromothenyl)guanine and 378 mg (0.5 mmol) of 10-bromodecyltetra-*O*-benzoyl-*β*-d-glucopyranoside. Flash chromtatography (4.5 × 25 cm) with petroleum ether/acetone (3:2) gave pure **21** (142 mg, 35.8%). $C_{54}H_{54}BrN_5O_{11}S$ (1061.02); TLC: R_f 0.37 (SiO_2, acetone/petroleum ether 1:1); ESI-MS: *m/z* (% int.) 1060.2/1062.2 (80/100) $[M(^{79}Br/^{81}Br) + H]^+$ (calc. 1060.23/1062.23).

12-[*O*^{6}-(4-Bromothenyl)guan-9-yl]dodecyl-*β*-d-tetra-*O*-benzoylglucoside (23). The reaction was carried out with 163 mg (0.5 mmol) of *O*^{6}-(4-bromothenyl)guanine and 421 mg (0.5 mmol) of 12-bromododecyltetra-*O*-benzoyl-*β*-d-glucopyranoside. The raw product was used without purification for step C.

4-[O^6-(4-Bromothenyl)guan-9-yl]but-2-ynyl-*β*-d-tetra-*O*-acetylglucoside (25). The reaction was carried out with 163 mg (0.5 mmol) of *O*^{6}-(4-bromothenyl)guanine and 240 mg (0.5 mmol) of 4-bromobut-2-ynyltetra-*O*-acetyl-*β*-d-glucopyranoside. Flash chromatography (3 × 20 cm) with ethyl acetate/petroleum ether (2:1) gave pure **25** (135 mg, 37.3%). $C_{29}H_{30}BrN_5O_{11}S$ (724.54); TLC: R_f 0.53 (SiO_2, acetone/petroleum ether 1:1); HPLC (method II): R_t = 14.8 min; ESI-MS: *m/z* (% int.) 725.5/727.5 (88/100) $[M(^{79}Br/^{81}Br) + H]^+$ (calc. 724.09/726.09).

^{1}H NMR δ_H (250 MHz, $CDCl_3$, selected data): 4.395 (t, 2H, Alk1); 4.723 (d, Glc1); 4.876 (t, 2H, Alk4); 5.019 (br s, 2-NH_2); 5.653 (d, 2H, BT6); 7.115 (dt, BT3), 7.190 (d, BT5), 7.756 (s, G8); ^{1}H *J* couplings: 7.88 (Glc1,2); 1.9 (Alk1,4).

^{13}C NMR δ_C (62.9 MHz, $CDCl_3$, selected data): 32.93 (Alk4); 55.94 (Alk1); 61.79 (BT6); *79.91* (Alk2); *80.67* (Alk3); 98.30 (Glc1); 109.12 (BT4); 115.29 (G5); 124.04 (BT5); 130.85 (BT3); 138.60 (G8); 139.67 (BT2); 153.83 (G4); 159.09 (G2); 160.28 (G6).

2-(8-Aza-*O*^{6}-benzyl-guan-9-yl)ethyl-*β*-d-tetra-*O*-acetylglucoside (27). The reaction was carried out with 121 mg (0.5 mmol) of 8-aza-*O*^{6}-benzylguanine and 225 mg (0.5 mmol) of 2-bromoethyltetra-*O*-acetyl-*β*-d-glucopyranoside. Column chromatography (3 × 20 cm) with a stepwise applied gradient of ethyl acetate/petroleum ether (2:1, 3:1, 4:1) gave pure **27 (**61 mg, 19.8%). $C_{27}H_{32}N_6O_{11}$ (616.58); TLC: R_f 0.32 (SiO_2, acetone/petroleum ether 1:1); HPLC (method II): R_t = 13.5 min; ESI-MS: *m/z* (% int.) 617.2 (40) $[M + H]^+$ (calc. 617.22), 639.1 (20) $[M + Na]^+$, 1233.7 (100) $[2M + H]^+$, 1255.6 (20) $[2M + Na]^+$.

^{1}H NMR δ_H (250 MHz, $CDCl_3$, selected data): 4.091 (ddd, Alk1b); 4.288 (ddd, Alk1a); 4.471 (d, Glc1); 4.565 (ddd, Alk2b); 4.666 (ddd, Alk2a); 5.478 (br s, 2H, 2-NH_2); 5.601 (d, Bn7b); 5.623 (d, Bn7a); ^{1}H *J* couplings: 7.88 (Glc1,2); −10.5 (Alk1a,-1b); 5.1 (Alk1a,2a); 4.8 (Alk1a,2b); 7.85 (Alk1b,2a); 4.77 (Alk1b,2b); −14.5 (Alk2a,2b); −12.2 (Bn7a,7b).

^{13}C NMR δ_C (62.9 MHz, $CDCl_3$, selected data): 45.68 (Alk2); 67.06 (Alk1); 68.79 (Bn7); 70.77 (Glc2); 100.48 (Glc1); 121.69 (G5); 128.30 (Bn4); 128.36 (Bn3,5); 128.45 (Bn2,6); 135.48 (Bn1); 153.56 (G4); *161.63* (G6); *161.76* (G2).

Deprotection of the Nucleoside Analogues (12, 14, 16, 18, 20, 22, 24, 26, and 28). For removal of acetyl or benzoyl groups (Chart 2, step C), 1 equiv of the nucleoside analogue was dissolved in methanol (2 mL/mmol), and 0.1 equiv of a freshly prepared 0.1 M sodium methanolate solution was added. The reaction was monitored by TLC. The mixture was neutralized with Dowex (H^+ 50WX2) ion exchanger and filtered. The solvent was evaporated from the filtrate, and the final product was purified by flash chromatography and, if possible, by recrystallization. Note: compound **24** was synthesized without purification of the protected glucoside **23**. The reaction mixture from step B was directly dissolved and used for step C since good separation of N9 and N7 derivatives was possible in the deprotected form (see Results). Detailed analytical results and complete NMR data are presented as Supporting Information.

Supporting Information Available: Tables A1−A7, detailed interaction energies between each amino acid residue in the MGMT binding region and each structural segment of the inhibitors shown in Tables 3 and 4; Table B, details of the HPLC purifications, yields, and UV absorption data for 4-BTG (**10**) and the inhibitors **12**−**28**; additional detailed ^{1}H and ^{13}C NMR data and assignments for the precursor glycosides **2**, **3**, **5**, and **6** and for the protected nucleosides **11**, **15**, **17**, **21**, and **23** in Table C; complete ^{1}H and ^{13}C NMR chemical shift data with assignments for the inhibitors **12**, **14**, **16**, **18**, **20**, **22**, **24**, **26**, **28** in Tables D and E, respectively; and diagnostic J_{CH} and J_{HH} of useful structural information in Tables F and G, respectively.

References

(1) D'Incalci, M.; Citti, L.; Taverna, P.; Catapano, C. V. Importance of the DNA repair enzyme *O*^{6}-alkyl guanine alkyltransferase (AT) in cancer chemotherapy. *Cancer Treat. Rev.* **1988**, *15*, 279−292.

(2) Pegg, A. E.; Byers, T. L. Repair of DNA containing *O*^{6}-alkylguanine. *FASEB J.* **1992**, *6*, 2302−2310.

(3) Mitra, S.; Kaina, B. Regulation of repair of alkylation damage in mammalian genomes. *Prog. Nucleic Acid Res. Mol. Biol.* **1993**, *44*, 109−142.

(4) Pegg, A. E.; Dolan, M. E.; Moschel, R. C. Structure, function, and inhibition of *O*^{6}-alkylguanine-DNA alkyltransferase. *Prog. Nucleic Acid Res. Mol. Biol.* **1995**, *51*, 167−223.

(5) Morimoto, K.; Dolan, M. E.; Scicchitano, D.; Pegg, A. E. Repair of *O*^{6}-propylguanine and *O*^{6}-butylguanine in DNA by *O*^{6}-alkylguanine-DNA alkyltransferases from rat liver and *E. coli*. *Carcinogenesis* **1985**, *6*, 1027−1031.

(6) Dolan, M. E.; Pegg, A. E.; Dumenco, L. L.; Moschel, R. C.; Gerson, S. L. Comparison of the inactivation of mammalian and bacterial *O*^{6}-alkylguanine-DNA alkyltransferases by *O*^{6}-benzylguanine and *O*^{6}-methylguanine. *Carcinogenesis* **1991**, *12*, 2305−2309.

(7) Dolan, M. E.; Mitchell, R. B.; Mummert, C.; Moschel, R. C.; Pegg, A. E. Effect of *O*^{6}-benzylguanine analogues on sensitivity of human tumor cells to the cytotoxic effects of alkylating agents. *Cancer Res.* **1991**, *51*, 3367−3372.

(8) McElhinney, R. S.; Donnelly, D. J.; McCormick, J. E.; Kelly, J.; Watson, A. J.; Rafferty, J. A.; Elder, R. H.; Middleton, M. R.; Willington, M. A.; McMurry, T. B. H.; Margison, G. P. Inactivation of *O*^{6}-alkylguanine-DNA alkyltransferase. 1. Novel *O*^{6}-(hetarylmethyl)guanines having basic rings in the side chain. *J. Med. Chem.* **1998**, *41*, 5265−5271.

(9) Chae, M. Y.; Swenn, K.; Kanugula, S.; Dolan, M. E.; Pegg, A. E.; Moschel, R. C. 8-Substituted *O*^{6}-benzylguanine, substituted 6(4)−(benzyloxy)pyrimidine, and related derivatives as inactivators of human *O*^{6}-alkylguanine-DNA alkyltransferase. *J. Med. Chem.* **1995**, *38*, 359−365.
(10) Dolan, M. E.; Pegg, A. E. *O*^{6}-benzylguanine and its role in chemotherapy. *Clin. Cancer Res.* **1997**, *3*, 8837−847.
(11) Friedman, H. S.; Kokkinakis, D. M.; Pluda, J.; Friedman, A. H.; Cokgor, I.; Haglund, M. M.; Ashley, D. M.; Rich, J.; Dolan, M. E.; Pegg, A. E.; Moschel, R. C.; McLendon, R. E.; Kerby, T.; Herndon, J. E.; Bigner, D. D.; Schold, S. C., Jr. Phase I trial of *O*^{6}-benzylguanine for patients undergoing surgery for malignant glioma. *J. Clin. Oncol.* **1998**, *16*, 3570−3575.
(12) Roy, S. K.; Moschel, R. C.; Dolan, M. E. Pharmacokinetics and metabolism in rats of an inactivator of *O*^{6}-alkylguanine-DNA alkyltransferase. *Drug Metab. Dispos.* **1996**, *24*, 1205−1211.
(13) Middleton, M. R.; Kelly, J.; Thatcher, N.; Donnelly, D. J.; McElhinney, R. S.; McMurry, T. B.; McCormick, J. E.; Margison, G. P. *O*^{6}-(4-bromothenyl)guanine improves the therapeutic index of Temozolomide against A375M melanoma xenografts. *Int. J. Cancer* **2000**, *85*, 248−252.
(14) Dolan, M. E.; Stine, L.; Mitchell, R. B.; Moschel, R. C.; Pegg, A. E. Modulation of mammalian *O*^{6}-alkylguanine-DNA alkyltransferase in vivo by *O*^{6}-benzylguanine and its effect on the sensitivity of a human glioma tumor to 1-(2-chloroethyl)-3-(4-methylcyclohexyl)-1-nitrosourea. *Cancer Commun.* **1990**, *2*, 371−377.
(15) Mitchell, R. B.; Moschel, R. C.; Dolan, M. E. Effect of *O*^{6}-benzylguanine on the sensitivity of human tumor xenografts to 1, 3-bis(2-chloroethyl)-1-nitrosourea and on DNA interstrand cross-link formation. *Cancer Res.* **1992**, *52*, 1171−1175.
(16) Moschel, R. C.; McDougall, M. G.; Dolan, M. E.; Stine, L.; Pegg, A. E. Structural features of substituted purine derivatives compatible with depletion of human *O*^{6}-alkylguanine-DNA alkyltransferase. *J. Med. Chem.* **1992**, *35*, 4486-4491.
(17) Chae, M. Y.; McDougall, M. G.; Dolan, M. E.; Swenn, K.; Pegg, A. E.; Moschel, R. C. Substituted *O*^{6}-benzylguanine derivatives and their inactivation of human *O*^{6}-alkylguanine-DNA alkyltransferase *J. Med. Chem.* **1994**, *37*, 342−347.
(18) Mineura, K.; Fukuchi, M.; Kowada, M.; Terashima, I.; Kohda, K. Differential inactivation of *O*^{6}-methylguanine-DNA methyltransferase activity by *O*^{6}-arylmethylguanines. *Int. J. Cancer* **1995**, *63*, 148−151.
(19) Dolan, M. E.; Roy, S. K.; Garbiras, B. J.; Helft, P.; Paras, P.; Chae, M. Y.; Moschel, R. C.; Pegg, A. E. *O*^{6}-alkylguanine-DNA alkyltransferase inactivation by ester prodrugs of *O*^{6}-benzylguanine derivatives and their rate of hydrolysis by cellular esterases. *Biochem. Pharmacol.* **1998**, *55*, 1701−1709.
(20) Abril, N.; Luque, R. F.; Prieto, A. M.; Rafferty, J. A.; Margison, G. P.; Pueyo, C. Bacterial and mammalian DNA alkyltransferases sensitize *Escherichia coli* to the lethal and mutagenic effects of dibromoalkanes. *Carcinogenesis* **1997**, *18*, 1883−1888.
(21) Pegg, A. E.; Chung, L.; Moschel, R. C. Effect of DNA on the inactivation of *O*^{6}-alkylguanine-DNA alkyltransferase by 9-substituted *O*^{6}-benzylguanine derivatives. *Biochem. Pharmacol.* **1997**, *53*, 1559−1564.
(22) Moore, M. H.; Gulbis, J. M.; Dodson, E. J.; Demple, B.; Moody, P. C. Crystal structure of a suicidal DNA repair protein: the Ada *O*^{6}-methylguanine-DNA methyltransferase from *E. coli*. *EMBO J.* **1994**, *13*, 1495−1501.
(23) Wibley, J. E.; McKie, J. H.; Embrey, K.; Marks, D. S.; Douglas, K. T.; Moore, M. H.; Moody, P. C. A homology model of the three-dimensional structure of human *O*^{6}-alkylguanine-DNA alkyltransferase based on the crystal structure of the C-terminal domain of the Ada protein from *Escherichia coli*. *Anticancer Drug Des.* **1995**, *10*, 75−95. [Erratum: *Anticancer Drug Des.* **1995**, 439].
(24) Vora, R. A.; Pegg, A. E.; Ealick, S. E. A new model for how *O*^{6}-methylguanine-DNA methyltransferase binds DNA. *Proteins* **1998**, *32*, 3−6.
(25) Brown, L. R.; Deng, J.; Clarke, N. D. Dominant sensitization variants of human *O*^{6}-methylguanine-DNA-methyltransferase obtained by a mutational screen of surface residues. *Mutat. Res. DNA Repair* **2000**, *459*, 81−87.
(26) Cheng, X. DNA modification by methyltransferases. *Curr. Opin. Struct. Biol.* **1995**, *5*, 4−10.
(27) Cheng, X.; Blumenthal, R. M. Finding a basis for flipping bases. *Structure* **1996**, *4*, 639−645.
(28) Klimasauskas, S.; Kumar, S.; Roberts, R. J.; Cheng, X. HhaI methyltransferase flips its target base out of the DNA helix. *Cell* **1994**, *76*, 357−369.
(29) Wibley, J. E.; Pegg, A. E.; Moody, P. C. Crystal structure of the human *O*^{6}-alkylguanine-DNA alkyltransferase. *Nucleic Acids Res.* **2000**, *28*, 393−401.
(30) Daniels, D. S.; Mol, C. D.; Arvai, A. S.; Kanugula, S.; Pegg, A. E.; Tainer, J. A. Active and alkylated human AGT structures: a novel zinc site, inhibitor and extrahelical base binding. *EMBO J.* **2000**, *19*, 1719−1730.
(31) Xu Welliver, M.; Pegg, A. E. Point mutations at multiple sites including highly conserved amino acids maintain activity but render *O*^{6}-alkylguanine-DNA alkyltransferase insensitive to *O*^{6}-benzylguanine *Biochem. J.* **2000**, *347*, 519−526.
(32) Kanugula, S.; Goodtzova, K.; Edara, S.; Pegg, A. E. Alteration of arginine 128 to alanine abolishes the ability of human *O*^{6}-alkylguanine-DNA alkyltransferase to repair methylated DNA but has no effect on its reaction with *O*^{6}-benzylguanine. *Biochemistry* **1995**, *34*, 7113−7119.
(33) Xu Welliver, M.; Kanugula, S.; Loktionova, N. A.; Crone, T. M.; Pegg, A. E. Conserved residue lysine-165 is essential for the ability of *O*^{6}-alkylguanine-DNA alkyltransferase to react with *O*^{6}-benzylguanine. *Biochem. J.* **2000**, *347*, 527−534.
(34) Goodtzova, K.; Kanugula, S.; Edara, S.; Pegg, A. E. Investigation of the role of tyrosine-114 in the activity of human *O*^{6}-alkylguanine-DNA alkyltransferase. *Biochemistry* **1998**, *37*, 12489−12495.
(35) Xu, W. M.; Leitao, J.; Kanugula, S.; Pegg, A. E. Alteration of the conserved residue tyrosine-158 to histidine renders human *O*^{6}-alkylguanine-DNA alkyltransferase insensitive to the inhibitor *O*^{6}-benzylguanine. *Cancer Res.* **1999**, *59*, 1514−1519.
(36) Xu, W. M.; Leitao, J.; Kanugula, S.; Meehan, W. J.; Pegg, A. E. Role of codon 160 in the sensitivity of human *O*^{6}-alkylguanine-DNA alkyltransferase to *O*^{6}-benzylguanine. *Biochem. Pharmacol.* **1999**, *58*, 1279−1285.
(37) Pohl, J.; Bertram, B.; Hilgard, P.; Nowrousian, M. R.; Stuben, J.; Wiessler, M. D-19575−a sugar-linked isophosphoramide mustard derivative exploiting transmembrane glucose transport. *Cancer Chemother. Pharmacol.* **1995**, *35*, 364−370.
(38) Veyhl, M.; Wagner, K.; Volk, C.; Gorboulev, V.; Baumgarten, K.; Weber, W. M.; Schaper, M.; Bertram, B.; Wiessler, M.; Koepsell, H. Transport of the new chemotherapeutic agent beta-d-glucosylisophosphoramide mustard (D-19575) into tumor cells is mediated by the Na^+-d-glucose cotransporter SAAT1. *Proc. Natl. Acad. Sci. U.S.A.* **1998**, *95*, 2914−2919.
(39) Reinhard, J.; Eichhorn, U.; Wiessler, M.; Kaina, B. Inactivation of *O*^{6}-methylguanine-DNA methyltransferase (MGMT) by glucose-conjugated inhibitors. *Int. J. Cancer* **2001**, in press.
(40) Balsinger, R. W.; Montgomery, J. A. Synthesis of potential anticancer agents. XXV. Preparation of 6-alkoxy-2-aminopurines. *J. Org. Chem.* **1960**, *25*, 1573−1575.
(41) Shealy, Y. F.; Clayton, J. D.; O'Dell, C. A.; Montgomery, J. A. *v*-Triazolo[4, 5-*d*]pyrimidines. II. *O*-substituted derivatives of 8-aza-guanine and 8-aza-hypoxanthine. *J. Org. Chem.* **1962**, *27*, 4518−4523.
(42) O'Brien, D. E.; Cheng, C. C.; Pfleiderer, W. Pyrimidines. XVIII. 2,4-diamino-5-nitro-6-arylaminopyrimidines. Nitration study of 2,4-diamino-6-chloropyrimidine and a literature correction. *J. Med. Chem.* **1966**, *9*, 573−575.
(43) Kjellberg, J.; Liljenberg, M. Regioselective alkylation of 6-(*β*-methoxyethoxy)guanine to give the 9-alkylguanine derivative. *Tetrahedron Lett.* **1986**, *27*, 877−880.
(44) Davis, B. M.; Roth, J. C.; Liu, L.; Xu, W. M.; Pegg, A. E.; Gerson, S. L. Characterization of the P140K, PVP(138−140)MLK, and G156A *O*^{6}-methylguanine-DNA methyltransferase mutants: implications for drug resistance gene therapy. *Hum. Gene Ther.* **1999**, *10*, 2769−2778.
(45) Preuss, I.; Haas, S.; Eichhorn, U.; Eberhagen, I.; Kaufmann, M.; Beck, T.; Eibl, R. H.; Dall, P.; Bauknecht, T.; Hengstler, J.; Wittig, B. M.; Dippold, W.; Kaina, B. Activity of the DNA repair protein *O*^{6}-methylguanine-DNA methyltransferase in human tumor and corresponding normal tissue. *Cancer Detect. Prev.* **1996**, *20*, 130−136.
(46) Paulsen H. Fortschritte bei der selektiven chemischen Synthese verzweigter Oligosaccharide. *Angew. Chem.* **1982**, *94*, 184−201.
(47) Helferich, B.; Zirner, J. Notiz über Tetraacetyl-[4-brom-*n*-butyl]-*β*-d-glucosid. *Chem. Ber.* **1962**, *96*, 374.

JM010006E